Crystalline 1D Heterocyclic Quinoidal Conjugated Polymers as Catalysts for Facilitating the Oxygen Reduction Reaction

Renzhen Fan, Cheng Wang, Xiaofei Zhang, Xuwen Zhang, Weijia Dong, Yiyang Xu, Chenhui Xu,

Chunyan Chi, Jun Zhu,* Yunfeng Deng* and Yanhou Geng*

Abstract: The pursuit of cost-effective and efficient metal-free electrocatalysts for advancing the oxygen reduction reaction (ORR) is essential for the progress of energy conversion and storage technologies. In this study, we present the synthesis of a series of crystalline one-dimensional (1D) heterocyclic quinoidal conjugated polymers characterized by tight π-stacking, a small bandgap, commendable charge carrier mobility, favorable film-forming properties, and excellent stability. The optoelectronic properties of these polymers are fine-tuned through the introduction of additional heteroatoms and/or substituents in the monomers and comonomers to understand and optimize their ORR catalytic activity. Evaluation of their catalytic performances, aided by theoretical computations, revealed a remarkable half-wave potential and limiting current density of up to 0.74 V and 7.50 mA cm^{-2}, respectively. Our research not only provides valuable insights into the design of 1D polymers but also extends its implications to other type of organic systems, offering a strategy for enhancing ORR catalytic performance.

The oxygen reduction reaction (ORR) is a pivotal process in the development of sustainable and clean energy conversion and storage systems, such as metal-air batteries and proton-exchange membrane fuel cells. However, progress in these technologies has been impeded by the sluggish kinetics of the ORR. Currently, commercially available catalysts for the ORR primarily consist of precious platinum-based materials. Nevertheless, their high cost, scarcity, poor stability, and detrimental environmental effects hinder their widespread adoption. Thus, the quest for alternative and innovative ORR catalysts is not only crucial but also poses a great challenge.

Metal-free catalysts, including synthetic porous organic polymers, as well as natural polymers like cellulose, chitosan, and alginate, have received significant research attention due to their distinctive structural features, providing excellent structural stability and processability. Despite these advantages, the majority of pure polymer materials inherently exhibit negligible oxygen reduction reaction (ORR) catalytic activity, attributed to their poor conductivity and lack of active sites for the reaction. Nevertheless, the pyrolysis and heteroatom doping methods have demonstrated considerable promise in enhancing ORR performance. However, these methods come with inherent drawbacks, including additional energy consumption, substantial weight loss (typically exceeding 60%), and creation of uncontrollable and undefined active sites at the atomic level. These limitations hamper a comprehensive understanding of the intrinsic ORR electrocatalytic mechanism.

While there has been extensive research on the ORR catalytic performance of crystalline two-dimensional (2D) and three-dimensional (3D) organic polymers, the investigation of one-dimensional (1D) linear polymers is relatively nascent. This is primarily due to the tendency of 1D polymers to adopt an amorphous phase during preparation, posing challenges for an in-depth understanding of their ORR catalytic mechanism. Nevertheless, in recent years, there has been a growing exploration of 1D linear conjugated polymers with characteristics such as tight π-stacking, a small bandgap, high charge carrier mobility, good film-forming properties, and excellent stability, particularly in the realm of energy conversion applications. The distinctive feature of conjugated 1D polymers lies in their intrinsic electrical conductivity and easily adjustable local heteroatomic composition. Moreover, the intramolecular and intermolecular interactions, along with strong dipole interactions, significantly enhance charge transport and diffusion through the conjugated backbones. Generally, five-membered and six-membered ring heterocycles have proven to be the preferred building blocks for efficient ORR catalysts. This preference arises from the ease with which the sp^2-hybridization of the carbon center can be disrupted by introducing heteroatoms with lone pairs of electrons, thereby altering the local spin density and charge distributions within the conjugated structures. With the above-mentioned design strategy in mind, herein we synthesized a series of crystalline 1D heterocyclic quinoidal conjugated polymers and revealed their potential as efficient catalysts for facilitating the ORR in fuel cell applications.

These polymers were synthesized via Stille polymerization utilizing a heterocyclic quinoidal monomer paired with a bithiazole comonomer. The compelling intermolecular interactions, stemming from the electron-deficient quinoidal monomer and the electron-rich bithiazole comonomer, resulted in a notable degree of crystallinity for these 1D polymers. Furthermore, these polymers exhibit small bandgaps attributed to the intramolecular donor-acceptor interactions. Meanwhile, the HOMO and LUMO orbitals are delocalized across the backbone, which can promote intramolecular charge transfer through the conjugated structure. Notably, the low LUMOs of these polymers and the more positively charged carbon active sites adjacent to heteroatoms can largely facilitate efficient O_2 adsorption and enhance the ORR process. Additionally, these polymers exhibit remarkable stability and excellent processability. When cast into thin films, they manifest a charge carrier mobility of up to xxx. These distinctive characteristics render these polymers highly promising for applications in the ORR process.

For a more comprehensive study, the electronic properties of the polymer backbones were fine-tuned by introducing additional heteroatoms and/or substituents in the monomers and comonomers to understand and optimize their ORR performance. Subsequently, the catalytic performance of the resulting polymers was assessed, assisted by theoretical

computations. The results revealed a remarkable halfwave potential and limiting current density of up to 0.74 V and 7.50 mA cm^{-2}, respectively. Our research offers insights into the design of not only 1D polymers but also 2D and 3D organic systems to enhance ORR catalytic performance.

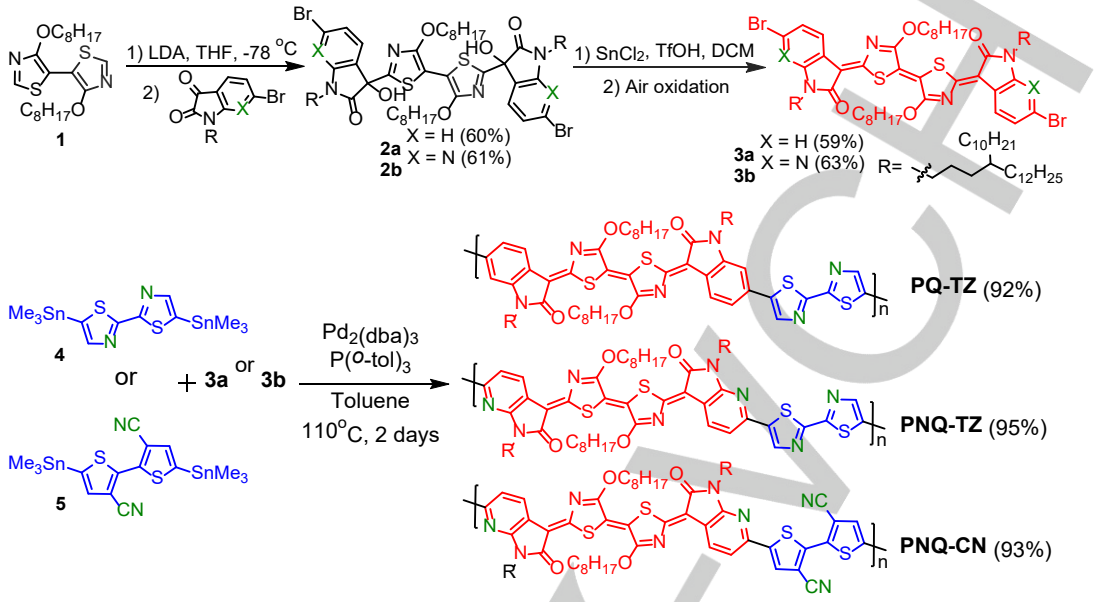

Scheme 1. Synthetic route for **PQ-TZ**, **PNQ-TZ** and **PNQ-CN**.

The synthesis details are elucidated in Scheme 1, wherein carefully chosen starting materials with inherent N and/or S heteroatoms were employed. The initial step involved treating bithiazole compound **1** with lithium diisopropylamide (LDA) for proton abstraction. Nucleophilic addition of indole-2,3-dione led to the crucial dihydroxyl precursors, **2a** and **2b**. Subsequent treatment of these precursors with Tin dichloride and triflic acid generated diradical intermediates. These intermediates, upon oxidation in air, transformed into the fully conjugated electron-deficient quinoidal monomers **3a** and **3b**. Subsequently, the electron-rich bithiazoles, **4** and **5** were copolymerized with **3a** or **3b** by Stille coupling reaction to afford crude polymers, **PQ-TZ**, **PNQ-TZ** and **PNQ-CN**. The crude polymers were further purified by gel permeation chromatography using chloroform as the eluent, and the purified polymers were obtained by precipitation in methanol as black solids. The number average molecular weights (M_n) of **PQ-TZ**, **PNQ-TZ** and **PNQ-CN** were determined to be 16.1, 10.1 and 64.0 kDa, respectively, with a small polymer polydispersity index (PDI) of 1.2, 1.92 and 1.59, indicating uniform molecular weight distributions. Results of elemental analysis showed that the carbon (C), nitrogen (N) and sulphur (S) compositions closely matched the theoretical contents (Table SX), and there is no Palladium (Pd) residue observed in the polymer. Besides, all three polymers exhibited good thermal stability with thermal decomposition temperature (T_d) of above 310 ℃ (Figure SX).

The presence of the long alkyl chains in these polymers bestows exceptional processability upon them, facilitating easy casting onto desired substrates for diverse characterizations. The crystalline nature of the polymers was elucidated through experimental thin film X-ray diffraction patterns (Figure 1a-c) obtained by casting onto a zero-background silicon plate. The distinct reflections at 3.59° and 25.21° for **PQ-TZ**, 3.49° and 25.49° for **PNQ-TZ**, and 3.49° and 25.12° for **PNQ-CN** can be attributed to the (100) plane and (001) plane, respectively, which are characteristic of lamellar packing and π-stacking in such 1D polymers. There is a high degree of agreement between the simulated solid-state packings (Figure 1d-f) and the experimentally measured patterns. Pawley refinement was employed, yielding unit cell parameters of a = 25.55 Å, b = 13.51 Å, c = 3.53 Å, α = 134.78°, β =104.84°, γ =75.52°, with agreement factors of R_{wp} = 3.43%, R_p = 2.68%, for **PQ-TZ**; a = 25.54 Å, b = 9.83 Å, c = 3.49 Å, α = 124.55°, β =105.16°, γ =79.73°, with agreement factors of R_{wp} = 4.79%, R_p = 3.46%, for **PNQ-TZ**; a = 25.72 Å, b = 9.12 Å, c = 3.54 Å, α = 117.42°, β =104.57°, γ =83.04°, with agreement factors of R_{wp} = 3.43%, R_p = 2.68%, for **PNQ-CN**. These results demonstrated long-range order of the polymers with strong intermolecular interactions indicated by their small π-stacking distances (3.53, 3.49, and 3.54 Å, respectively for **PQ-TZ**, **PNQ-TZ** and **PNQ-CN**). In the simulated packing structures (Figure 1d-f), the aromatic polymer chains adopted a staggered stacking to maximize the interchain interactions, which is pivotal for the formation of well-defined 1D ordered polymers. Atomic force microscopy (AFM) images (Figure 1g-i) revealed uniform surfaces for the polymers when cast as thin films on a silicon wafer.

The UV-Vis absorption spectra of **PQ-TZ**, **PNQ-TZ**, and **PNQ-CN** were acquired by casting each respective polymer onto a transparent glass slide. Evidently, all three polymers exhibit pronounced absorption, initiating at 400 nm and extending to 1200 nm (Figure SX), implying efficient intramolecular charge transfer through the fully conjugated backbones. Cyclic voltammetry (CV) of **PQ-TZ**, **PNQ-TZ**, and **PNQ-CN** showed irreversible oxidation waves with onset at 0.84, 1.08 and 1.08 V respectively, with respect to SCE (Figure SX). The relatively

high oxidation potential and irreversible oxidative waves could be due to the electron deficient polymer backbones. On the contrary, reversible reduction waves with onset at -0.67, -0.71 and -0.51 V, respectively, with respect to SCE, were observed. With reference to ferrocene, the LUMO/HOMO energy levels were determined to be -3.73/-5.24, -3.69/-5.48, and -3.89/-5.48

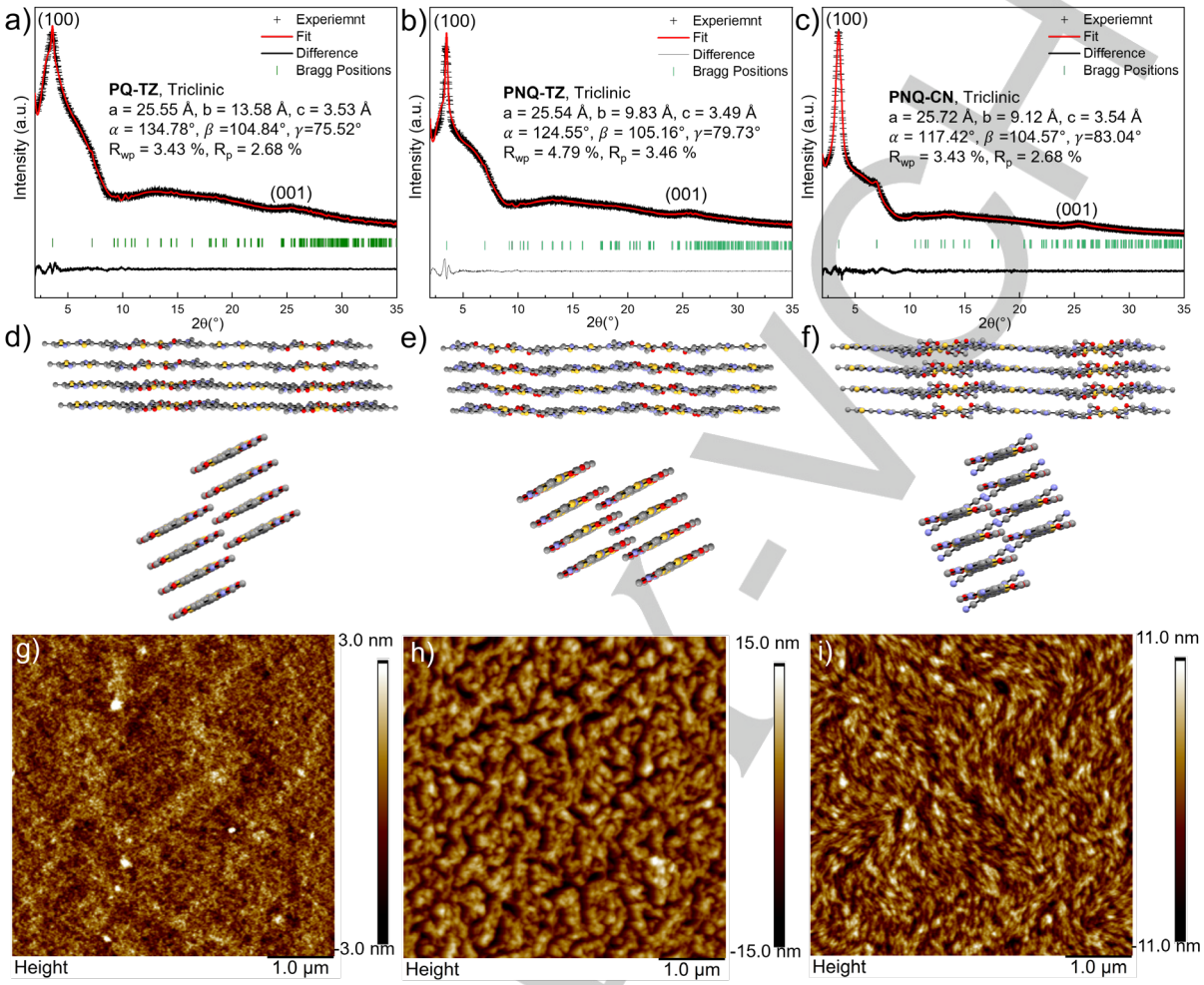

Figure 1. Pawley refinement of the experimental thin film X-ray diffraction pattern of (a) **PQ-TZ**, (b) **PNQ-TZ** and (c) **PNQ-CN** collected at room temperature; Front and side views of the simulated solid-state packing of (d) **PQ-TZ**, (e) **PNQ-TZ** and (f) **PNQ-CN**; AFM images of (g) **PQ-TZ**, (h) **PNQ-TZ** and (i) **PNQ-CN** spin-coated on a silica substrate.

eV, respectively. Hence, their energy gaps were obtained to be 1.51, 1.79 and 1.59 ev. Charge carrier mobilities of the polymers were measured by fabricating the polymers into thin film transistors. The results showed that xxxxxx (Figure SX, Table SX). These features make **PQ-TZ**, **PNQ-TZ**, and **PNQ-CN** promising for ORR electrochemical catalysis.

Each respective polymer was cast onto a glassy carbon electrode for the investigation of their ORR activities. Firstly, cyclic voltammetry (CV) curves of **PQ-TZ**, **PNQ-TZ** and **PNQ-CN** electrodes were obtained in nitrogen- and oxygen-saturated 0.1 M KOH aqueous electrolyte (Figure SX). No obvious redox wave was identified at 0.2-1.2 V (vs. RHE) under nitrogen-saturated condition for all three polymers. In contrast, a distinct reduction wave around 0.6-0.8 V (vs. RHE) can be observed in the oxygen-saturated electrolyte, indicating the electroactive nature of **PQ-TZ**, **PNQ-TZ** and **PNQ-CN** in facilitating the ORR process. Comparing the reduction waves of **PQ-TZ**, **PNQ-TZ** and **PNQ-CN** (Figure SX), **PNQ-TZ** exhibited a more positive potential for oxygen reduction, followed by **PQ-TZ** and **PNQ-CN**, implying their different ability to facilitate the ORR process. Subsequently, their linear sweep voltammetry (LSV) curves were obtained at different rotation rates (400 to 2500 rpm) in oxygen-saturated 0.1 M KOH aqueous electrolyte (Figure SX). The half-wave potentials of **PQ-TZ**, **PNQ-TZ** and **PNQ-CN** were determined to be 0.69, 0.74, and 0.71 V (vs. RHE) with limiting current densities of 4.97, 7.50and 6.18 mA cm^{-2}, respectively, from their LSV curves measured at 1600 rpm (Figure 2a). The relatively high half-wave potentials and large limiting current densities illustrate good ORR activity of these polymers. Among them, the more positive halfwave potential of **PNQ-TZ** (0.74 V), again, reveals its more efficient ORR activity, followed by **PQ-TZ** and **PNQ-CN**. The corresponding electron transfer number (n) of **PQ-TZ**, **PNQ-TZ** and **PNQ-CN** extracted from Koutecky-Levich (K-L) plots at 0.7 V were 3.43, 3.85, and 3.78, respectively (Figure SX), indicating a $4e^-$ transfer pathway in the ORR

process. The Tafel slopes derived from LSV curves were 82.6, 67.4, and 74.3 mV dec^{-1}, respectively for **PQ-TZ**, **PNQ-TZ** and **PNQ-CN** (Figure 2b). The smaller Tafel slope of **PNQ-TZ** (67.4 mV dec^{-1}) indicates its faster ORR kinetics, followed by **PQ-TZ** and **PNQ-CN**. Subsequently, the turnover frequencies (TOFs) were calculated at 0.7 V vs. RHE to evaluate their intrinsic activities. The TOFs of **PQ-TZ**, **PNQ-TZ** and **PNQ-CN** were estimated to be 0.121, 0.315 and 0.196 s^{-1}, respectively (Figure 2c). The larger TOF value of 0.315 s^{-1} for **PNQ-TZ** indicates its higher active sites utilization efficiency, followed by **PQ-TZ** and **PNQ-CN**. The durability of these polymers was evaluated at 0.7 V vs. RHE for 50000 s (Figure 2d). There was a small current loss in the first 5000 s, after which the system was stabilized, and no further current loss was observed. Besides, the current densities were largely retained upon addition of methanol into the electrolyte solution at 20000 s at 0.7 V vs. RHE, indicating their excellent tolerance towards small organic molecule.

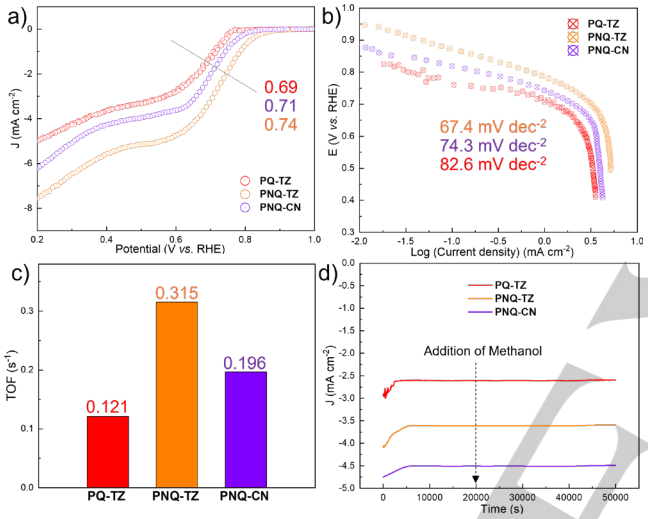

Figure 2. (a) LSV curves (at 1600 rpm) of **PQ-TZ**, **PNQ-TZ** and **PNQ-CN** (red, orange and purple) in O_2-saturated 0.1 M KOH electrolyte; (b) Comparison of Tafel plots of **PQ-TZ**, **PNQ-TZ** and **PNQ-CN**; (c) Comparison of the TOFs of **PQ-TZ**, **PNQ-TZ** and **PNQ-CN**; (d) Long-term stability test: current-time curve of of **PQ-TZ**, **PNQ-TZ** and **PNQ-CN** at 0.7 V vs. RHE.

DFT calculations were conducted to investigate and understand the ORR catalytic activities of **PQ-TZ**, **PNQ-TZ** and **PNQ-CN**. Firstly, the electrostatic potential surfaces (EPSs) of **PQ-TZ**, **PNQ-TZ** and **PNQ-CN** were obtained at the M06-2X/6-311G level (Figure 3a-c) for the identification of possible O_2 binding sites. The heteroatoms (especially O and N) in the polymers possess a strong negative electrostatic potential due to their high electronegativity, causing the nearby carbon atoms more electrostatically positive. Therefore, these nearby carbon sites could be possible active sites for ORR. Hirshfeld atomic charges were calculated at all atoms to qualitatively predict the most suitable ORR active carbon atom (Figure SX). A carbon with a large positive charge can lead to overly strong adsorption of oxygens and reaction intermediates, thus the subsequent reaction step cannot proceed (like site C2, C8, C17 and C24). Conversely, if the positive charge is too small, the initiation of the reaction can be challenging. Therefore, the carbons with appropriate positive charges are more prone to serve as the active catalytic sites. Furthermore, sulfur atoms (S) play a crucial role in boosting overall catalytic activity by finely tuning the local electron density distribution. Taking into account these distinctive features, it is plausible that sites C14 and C19 in the polymer backbones emerge as the most likely catalytic sites. The free energy diagram of **PQ-TZ**, **PNQ-TZ** and **PNQ-CN** were constructed to outline their overall ORR process. At U = 1.23 V, it can be observed that the O_2 → HOO* and HO* → OH^- are endothermic processes while HOO* → O* and O* → HO* steps are exothermic. The higher energy barrier of HO* → OH^- indicates it is the rate determine step in the ORR pathway. The overall energy barrier for **PQ-TZ**, **PNQ-TZ** and **PNQ-CN** were determined to be 0.59, 065 and 0.80 eV, respectively. The calculation results, again, confirmed the small energy barriers for these fully conjugated heterocyclic quinoidal polymers and the **PNQ-TZ** possess better catalytic efficiency, followed by **PQ-TZ** and **PNQ-CN**.

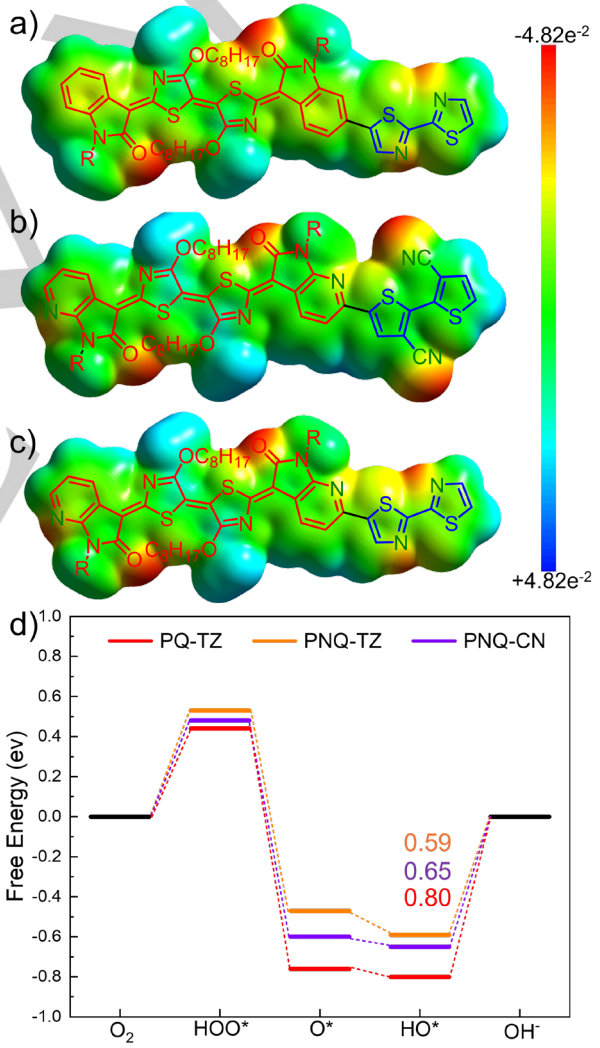

Figure 3. Electrostatic potential surfaces (EPS) of (a) **PQ-TZ,** (b) **PNQ-TZ** and (c) **PNQ-CN** (the long alky chains were replaced by methyl groups during calculation for simplicity and clarification). (d) Free energy diagram for **PQ-TZ**, **PNQ-TZ** and **PNQ-CN** at U=1.23 V (calculations were performed at site C14).

In summary, we have synthesized a series of crystalline 1D heterocyclic quinoidal conjugated polymers, featured by tight π-stacking, small bandgap, charge carrier mobility, good film-forming property as well as excellent stability. Their optoelectronic properties are fine-tuned by introducing additional heteroatoms and/or substituents in the monomers and comonomers for the optimization of their ORR catalytic activity. Their catalytic performances were assessed, assisted by theoretical computations. The results revealed a remarkable halfwave potential and limiting current density of up to 0.74 V and 7.50 mA cm^{-2}, respectively. Our research offers insights into the design of not only 1D polymers but also 2D and 3D organic systems to enhance ORR catalytic performance.

Acknowledgements

X. X. acknowledges XXX.

Keywords: 1 • 2 • 3 • 4 • 5

[1] a) X. Liu, D. Huang, C. Lai, G. Zeng, L. Qin, H. Wang, H. Yi, B. Li, S. Liu, M. Zhang, R. Deng, Y. Fu, L. Li, W. Xue, S. Chen, *Chem. Soc. Rev.* **2019**, 48, 5266-5302. b) X. Chen, K. Geng, R. Liu, K. T. Tan, Y. Gong, Z. Li, S. Tao, Q. Jiang, D. Jiang, *Angew. Chem. Int. Ed.* **2020**, 59, 5050-5091. c) S. Kandambeth, K. Dey, R. Banerjee, *J. Am. Chem. Soc.* **2019**, 141, 1807-1822. d) K. Geng, T. He, R. Liu, S. Dalapati, K. T. Tan, Z. Li, S. Tao, Y. Gong, Q. Jiang, D. Jiang, *Chem. Rev.* **2020**, 120, 8814-8933.

[2] a) X. Feng, X. Ding, D. Jiang, *Chem. Soc. Rev.* **2012**, 41, 6010-6022. b) J. W. Colson, W. R. Dichtel, *Nat. Chem* .**2013**, 5, 453-465. c) S. Y. Ding, W. Wang, *Chem. Soc. Rev.* **2013**, 42, 548-568.

[3]

Entry for the Table of Contents